Sphingolipid Levels and Processing of the Retinyl Chromophore in the Retina of a Mouse Model of Niemann-Pick Disease

Rahman, Bushra; Anderson, David M.G.; Chen, Chunhe; Liu, Jian; Migas, Lukasz G.; Van de Plas, Raf; Schey, Kevin L.; Kono, Masahiro; Fan, Jie; Koutalos, Yiannis

DOI
10.1167/iovs.65.14.24

Publication date
2024

Document Version
Final published version

Published in
Investigative ophthalmology & visual science

Sphingolipid Levels and Processing of the Retinyl Chromophore in the Retina of a Mouse Model of Niemann-Pick Disease

Bushra Rahman,[1] David M. G. Anderson,[2] Chunhe Chen,[1] Jian Liu,[1] Lukasz G. Migas,[3] Raf Van de Plas,[3] Kevin L. Schey,[2] Masahiro Kono,[1] Jie Fan,[1] and Yiannis Koutalos[1]

[1]Department of Ophthalmology, Medical University of South Carolina, Charleston, South Carolina, United States
[2]Mass Spectrometry Research Center and Department of Biochemistry, Vanderbilt University School of Medicine, Nashville, Tennessee, Unites States
[3]Delft Center for Systems and Control (DCSC), Delft University of Technology, Delft, Netherlands

Correspondence: Yiannis Koutalos, Department of Ophthalmology, Medical University of South Carolina, 167 Ashley Avenue, Charleston, SC 29425, USA; koutalo@musc.edu.

Received: July 18, 2024
Accepted: November 21, 2024
Published: December 11, 2024

Citation: Rahman B, Anderson DMG, Chen C, et al. Sphingolipid levels and processing of the retinyl chromophore in the retina of a mouse model of Niemann-Pick disease. *Invest Ophthalmol Vis Sci.* 2024;65(14):24. https://doi.org/10.1167/iovs.65.14.24

Purpose. Mutations in the gene that encodes the enzyme acid sphingomyelinase (ASMase) are associated with Niemann-Pick disease, a lysosomal storage disorder. Mice that lack ASMase (ASMase$^{-/-}$) exhibit age-related retinal degeneration and large increases in accumulation of lipofuscin in the retinal pigment epithelium (RPE). We examined which lipid species accumulate in the retina and the RPE of ASMase$^{-/-}$ mice and whether the retinal degeneration is associated with impaired photoreceptor metabolism and retinyl chromophore processing.

Methods. NADPH availability and all-*trans* retinol formation after rhodopsin bleaching were measured in isolated single rod photoreceptors with fluorescence imaging; sphingolipid levels in retinas and RPEs were measured with LC/MS; relative abundances of different lipid species in different retinal layers were measured with MALDI imaging mass spectrometry.

Results. There was no detectable difference in the kinetics of all-*trans* retinol formation or the NADPH-generating capacity between ASMase$^{-/-}$ and wild-type mice. Sphingomyelin levels were much higher in the retinas and RPEs of ASMase$^{-/-}$ animals compared to wild type, but there were no significant differences for ceramides. There was a large increase in the abundance of bis(monoacylglycero)phosphates (BMPs) in ASMase$^{-/-}$ mice, indicative of lysosomal dysfunction, but no substantial changes were detected for the *bis*-retinoid A2E.

Conclusions. Lysosomal dysfunction and retinal degeneration in ASMase$^{-/-}$ mice are not associated with defects in rod photoreceptor metabolism that affect all-*trans* retinol formation and availability of NADPH. Lysosomal dysfunction in ASMase$^{-/-}$ mice is not associated with *bis*-retinoid A2E accumulation.

Keywords: Niemann-Pick, retina, MALDI, fluorescence, sphingolipids

Lipofuscin consists of fluorescent pigment granules that accumulate with age as part of the lysosomal compartment of post-mitotic cells,[1,2] including those of the retinal pigment epithelium (RPE).[3] Because of its accumulation with age, lipofuscin has been hypothesized to play a role in age-related functional changes, including those associated with degenerative diseases, such as age-related macular degeneration (AMD).[4] A pathogenic role for lipofuscin is supported by its rapid accumulation in lysosomal storage disorders, a group of more than 70 diseases characterized by the intra-lysosomal accumulation of undegraded metabolites and caused by defects in lysosomal enzymes.[5,6] Niemann-Pick is one such lysosomal storage disorder disease, the A and B subtypes of which are caused by defects in acid sphingomyelinase (ASMase) activity that result in the lysosomal accumulation of sphingomyelin.[6,7] We have previously shown that in mice lacking ASMase, the ERG amplitude decreases and the retina degenerates with age, while there is a large accumulation of lipofuscin in the RPE, suggesting an association between lysosomal dysfunction, lipofuscin accumulation, and retinal pathology.[8]

The potential pathogenic role of lipofuscin has spurred studies on its composition, which however is likely to vary considerably across tissues. In the case of the RPE, the fluorophores responsible for the bulk of lipofuscin fluorescence originate in photoreceptor outer segments from reactions of the retinyl chromophore of the visual pigment.[1,9] More than 30 of these constituents of RPE lipofuscin have been identified to-date and classified as *bis*-retinoids.[10,11] The most abundant and best characterized *bis*-retinoid, A2E (N-retinylidene-N-retinylethanolamine),[12,13] has been shown to exhibit a range of cytotoxic properties, including the inhibition of lysosomal function.[14,15] *Bis*-retinoids originate in photoreceptor outer segments from the 11-*cis* and all-*trans*

isomers of retinal,[16–19] both of which are involved in the reactions underlying the detection of light. Detection of light begins with photoisomerization of the 11-*cis* retinyl chromophore of the visual pigment rhodopsin to all-*trans*, generating an active intermediate, but at the same time destroying rhodopsin.[20,21] Rhodopsin regeneration (reviewed in[22,23]) begins with the release of all-*trans* retinal by photoactivated rhodopsin, leaving behind the protein moiety opsin; fresh 11-*cis* retinal supplied to outer segments by RPE combines with opsin to reform rhodopsin[24]; the all-*trans* retinal released from photoactivated rhodopsin is reduced by retinol dehydrogenase RDH8 to all-*trans* retinol[25–27] using NADPH as cofactor[28]; and, finally, all-*trans* retinol leaves the outer segments and is transported to the RPE, where it is recycled to 11-*cis* retinal.

In view of the above, we hypothesized that the lysosomal dysfunction associated with lack of ASMase and accumulation of sphingomyelin would lead to impairment of retinal cell metabolism leading to degeneration. Impairment of rod photoreceptor metabolism would compromise the supply of NADPH and limit the reduction of the all-*trans* retinal released from photoactivated rhodopsin to all-*trans* retinol. We further hypothesized that the high levels of lipofuscin in the RPE of mice that lack ASMase[8] was the result of an increased accumulation of *bis*-retinoids due to the lysosomal dysfunction. An increase in *bis*-retinoid levels would also result from the impairment of rod photoreceptor metabolism, which would lead to build-up of all-*trans* retinal and the formation of *bis*-retinoid lipofuscin precursors. To test these hypotheses, we examined the reactions of the retinyl chromophore in the outer segments of single rod photoreceptors isolated from ASMase$^{-/-}$ mice and the abundance of sphingolipids and A2E in the retinas of ASMase$^{-/-}$ mice compared to wild type. We find that the formation of all-*trans* retinol, the availability of NADPH, and the levels of A2E in the RPE are unaffected in ASMase$^{-/-}$ mice compared to the wild type; sphingomyelin levels are much higher in the retinas and RPEs of ASMase$^{-/-}$ mice compared to wild type, as is the relative abundance of bis(monoacylglycero)phosphates (BMPs), which are associated with lysosomal dysfunction.[29–31] The results suggest that the visual dysfunction and retina degeneration in ASMase$^{-/-}$ mice are not associated with defects in photoreceptor metabolism that affect the processing of the visual pigment chromophore, or with increased accumulation of A2E in the RPE.

Methods

Animals

ASMase$^{-/-}$ mice were generated from breeding pairs of heterozygous ASMase$^{\pm}$ mice, a colony of which has been established from an original generous gift by Dr. Edward H. Schuchman. The background strain was C57BL/6. The offspring of the ASMase$^{\pm}$ breeding pairs were genotyped as previously described,[32] and 1-, 2-, and 6-month old ASMase$^{+/+}$ (wild type), ASMase$^{+/-}$ (heterozygote), and ASMase$^{-/-}$ (knockout) mice were used for experiments. All animal procedures were carried out in accordance with protocols approved by the Institutional Animal Care and Use Committee of the Medical University of South Carolina; the authors adhere to the ARVO Statement for the Use of Animals in Ophthalmic and Vision Research.

Single Cell Fluorescence Imaging

For experiments with isolated rod photoreceptor cells, two-month old animals were dark-adapted overnight and sacrificed under dim red light. The retinas were excised under either dim red or infrared light in mammalian physiological solution (in mmol/L: 130 NaCl, 5 KCl, 0.5 $MgCl_2$, 2 $CaCl_2$, 25 hemisodium-HEPES, 5 glucose, pH = 7.40), and fluorescence imaging experiments for determining NADPH availability and the kinetics of all-*trans* retinol formation were carried out as described previously.[33,34]

Kinetics of All-*Trans* Retinol Formation

The time-course of the outer segment fluorescence change after bleaching of rhodopsin was described with two rate constants, f_1 and f_2, corresponding to the formation and elimination of all-*trans* retinol, respectively,[34–36] with the outer segment fluorescence F due to all-*trans* retinol given by

$$F = f_1 \cdot A \cdot \left(e^{-f_2 t} - e^{-f_1 t}\right) / \left(f_1 - f_2\right) \quad (1)$$

where the parameter A is the outer segment fluorescence intensity that would correspond to the total amount of retinyl chromophore released by photoactivated rhodopsin. Values of the parameters A, f_1 and f_2 were determined for each cell by a least squares fit of the time course of the fluorescence intensity values using Origin software (OriginLab Corporation, Northampton, MA, USA). We reanalyzed the previously published results[34] for wild- type C57BL/6 mice in the same way to allow for a direct comparison. These published C57BL/6 all-*trans* retinol formation data provide a good wild type reference, because they were directly compared with biochemical and retinal slice measurements of all-*trans* retinol formation as well.[34] We did not characterize the kinetics of all-*trans* retinol formation in ASMase$^{+/+}$ C57BL/6 mice from the same litters as the ASMase$^{-/-}$ animals.

Rhodopsin Measurement

For determining the amount of rhodopsin in a mouse eye, the animal was sacrificed, and the eyes were enucleated under dim red light. An eye was hemisected at the level of the ora serrata, the anterior portion and the lens were removed, and the remaining posterior part of the eyecup was homogenized in PBS (in mmol/L: 10 sodium phosphate, 150 NaCl, pH 7.0). The tissue homogenate was then collected, leaving the eyecup sclera behind, and solubilized in 0.66% dodecyl maltoside in PBS. Hydroxylamine was added to a final concentration of 15 mM, and spectra were recorded between 250 and 700 nm with a Cary 300 spectrophotometer. The amount of rhodopsin was measured from the difference in the absorbance at 500 nm before and after bleaching the sample with >530 nm light.[37]

Sphingolipid Measurements With LC/MS

For determination of sphingolipid levels, one-, two-, and six-month old animals were dark-adapted overnight and sacrificed under dim red light. Eyes were enucleated and then hemisected at the level of the ora serrata in the mammalian physiological solution, and retinas were gently removed. After the removal of the retina, retinal pigment epithelial (RPE) cells were gently brushed off and collected with a transfer pipette. For each animal, the two retinas were

Investigative Ophthalmology & Visual Science

combined into one sample, and the two RPE cell collections into another. For each sample, the protein concentration was measured with the Novagen BCA Protein Assay Kit (Millipore Sigma, Burlington, MA, USA), and the levels of different sphingolipids were determined by LC/MS at the MUSC Lipidomics Core Facility.[8] Sphingolipid levels are reported as pmol lipid per mg protein. Experiments were repeated three times ($n = 3$).

MALDI Imaging Mass Spectrometry and Optical Imaging

For matrix-assisted laser desorption ionization imaging mass spectrometry (MALDI IMS), whole eyes from one-, two-, and six-month old ASMase$^{+/+}$, ASMase$^{+/-}$, and ASMase$^{-/-}$ animals were embedded by placing the eyes in 2.7% carboxymethylcellulose (Sigma Aldrich, St. Louis, MO, USA) in a polystyrene container and rapidly freezing the media with liquid nitrogen vapor.

Samples were then shipped to Vanderbilt, and sections were taken at 12 µm thickness using a Leica CM3050s cryostat (Leica, Wetzlar, Germany). The matrices, 2,5-dihydroxyacetophenone (DHA) and 1, 5-diaminonaphalene (DAN) were applied using a custom in house designed sublimation device for positive and negative ion mode analysis. Data were acquired on a timsTOF fleX platform (Bruker Daltonik, Bremen, Germany)[38] with methods optimized for a 5 and 10 µm pixel size. Data were acquired over m/z 300-2000 mass range with 200 shots per pixel for 10 µm experiments and 25 shots for 5 µm experiments. MALDI-IMS were generated using SCiLS software (Bruker Daltonik, Bremen, Germany). Tissues ran with a 5 µm pixels size were stained with hematoxylin and eosin after data acquisition and the optical images were registered with the MALDI IMS using image2image - Migas et al. (2023). image2image (version 0.1.6) [Computersoftware], https://github.com/vandeplaslab/image2image-docs.

Material

All reagents were of analytical grade.

Statistical Analysis

We used one- and two-factor ANOVA (with replication) to examine the effects of different variables, one- and two-tailed *t*-tests to test for differences between means, and linear regression to examine the effect of acyl chain length on the abundance of sphingomyelins and ceramides—for this last analysis, we included all species for each chain length regardless of the number of double bonds, and we excluded the C14 and C26 species as they had very low abundance. Results were considered statistically significant when $P < 0.05$, with a Bonferroni correction applied when multiple comparisons were carried out. The number of multiple comparisons in those cases was three, and so the level of statistical significance was adjusted to $P < 0.017$ (0.05/3).

Results

Kinetics of All-*Trans* Retinol Formation in ASMase$^{-/-}$ Mouse Rod Photoreceptors

After bleaching of rhodopsin in rod photoreceptors, there is a large increase in outer segment fluorescence >420 nm

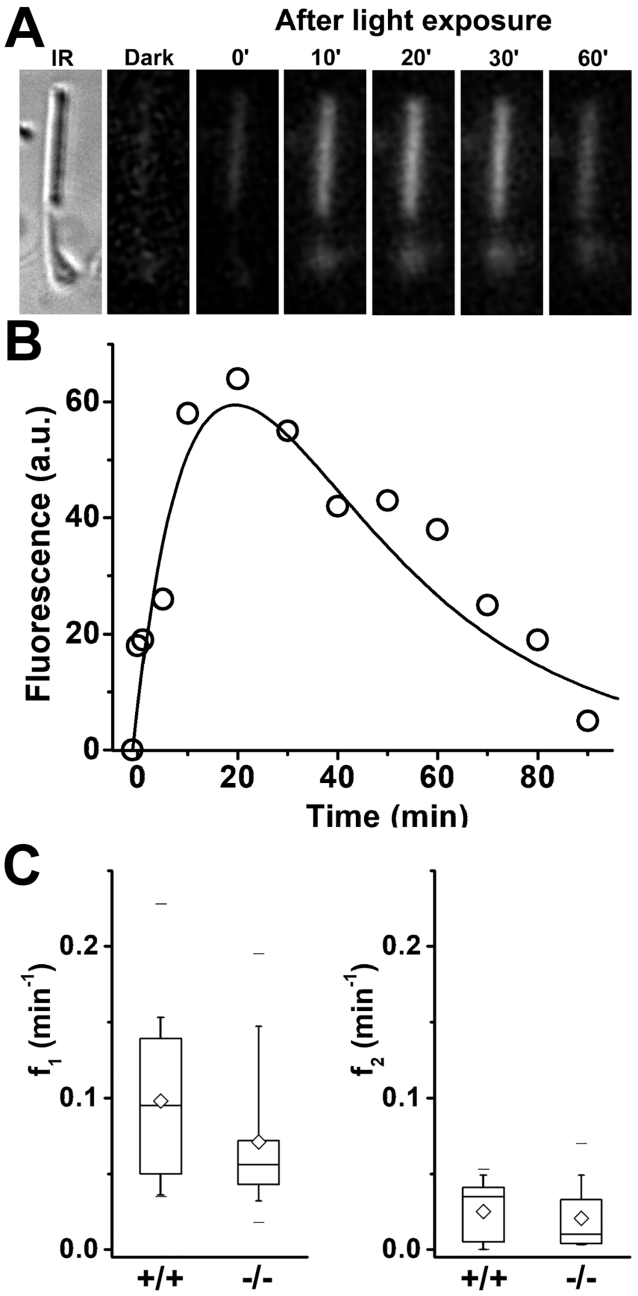

Figure 1. Formation of all-*trans* retinol in isolated rod photoreceptors from ASMase$^{-/-}$ mice. **(A)** Retinol fluorescence increases in the outer segment of an intact ASMase$^{-/-}$ rod photoreceptor after rhodopsin bleaching. IR, infrared image of the cell; fluorescence (excitation, 360 nm; emission, >420 nm) images of the cell before (*dark*) and at different times after bleaching. All fluorescence images are shown at the same intensity scaling. **(B)** Rod outer segment all-*trans* retinol fluorescence (*circles*) of the cell in **(A)** at different times after bleaching. Bleaching was carried out between t = −1 minute and t = 0. The *solid line* is a least squares fit of Equation 1, $f_1 \cdot A \cdot (e^{-f_2 t} - e^{-f_1 t})/(f_1 - f_2)$, through the data points, giving rate constants $f_1 = 0.069$ min^{-1} and $f_2 = 0.030$ min^{-1}. **(C)** Wild type (+/+, $n = 13$) and ASMase$^{-/-}$ (−/−, $n = 11$) rod photoreceptors have the same all-*trans* retinol formation and elimination rate constants, f_1 and f_2. *Box range*: 25%–75%; Whiskers: 5%–95%; Limits: Min/Max; Mean, ◇. All experiments carried out at 37°C.

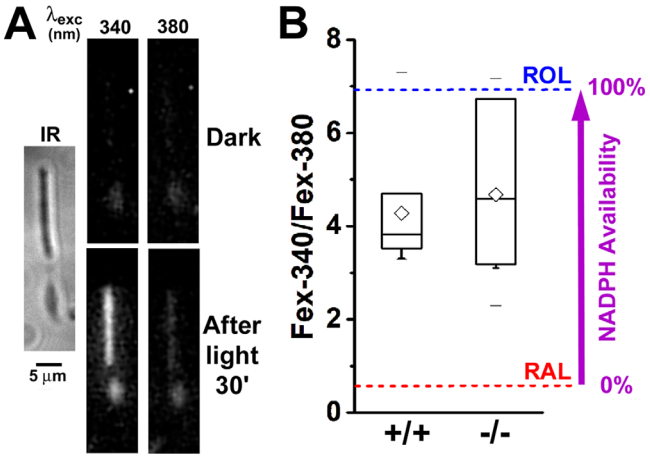

Figure 2. Comparison of the NADPH-generating capacity of ASMase$^{-/-}$ rod photoreceptors with wild type. (**A**) Measurement of NADPH-generating capacity of an isolated intact ASMase$^{-/-}$ rod from the conversion of all-*trans* retinal to all-*trans* retinol. Retinol and retinal were distinguished by exciting fluorescence with 340 and 380 nm light, and collecting emission for >420 nm. IR, infrared image of the cell; fluorescence images of the cell before (*dark*) and 30 minutes after bleaching are shown with the same intensity scaling to facilitate comparisons. (**B**) Wild-type (+/+, $n = 7$) and ASMase$^{-/-}$ (−/−, $n = 7$) rod photoreceptors have the same NADPH-generating capacity, as measured from the ratio Fex-340/Fex-380 of the fluorescence intensities excited by 340 and 380 nm light. Box range: 25%–75%; Whiskers: 5%–95%; Limits: Min/Max; Mean, ◊. The Fex-340/Fex-380 ratios for all-*trans* retinal (0.55, RAL) and all-*trans* retinol (6.95, ROL) represent the extremes of no conversion and of full conversion of retinal to retinol, respectively. Experiments carried out at 37°C.

(excited by 360 nm) that is due mostly to all-*trans* retinol formed from the reduction of all-*trans* retinal released by photoactivated rhodopsin.[33,34] In an ASMase$^{-/-}$ mouse rod photoreceptor, outer segment fluorescence rises rapidly after bleaching, reaching a peak in ~30 min, and then declines slowly as all-*trans* retinol leaves the outer segment (Fig. 1A). Figure 1B plots the fluorescence changes from the cell in Figure 1A. A least squares fit of the data with Equation 1, gave values of $f_1 = 0.069$ min^{-1} and $f_2 = 0.030$ min^{-1} for the all-*trans* retinol formation and elimination rate constants, and A = 117 for the amplitude. From $n = 11$ ASMase$^{-/-}$ rods, the average values for the formation and elimination rate constants were $f_1 = 0.071 \pm 0.051$ min^{-1} (mean ± SD) and $f_2 = 0.021 \pm 0.021$ min^{-1} (mean ± SD), respectively. The average values from $n = 13$ C57BL/6 rods,[34] obtained by analyzing the data in the same way, were $f_1 = 0.098 \pm 0.055$ min^{-1} (mean ± SD) and $f_2 = 0.025 \pm 0.019$ min^{-1} (mean ± SD). As shown in Figure 1C, the rate constants of the ASMase$^{-/-}$ cells were not significantly different from those of the wild type (two-tailed *t*-test, $P = 0.25$ and 0.61, for f_1 and f_2, respectively). The rhodopsin levels of dark-adapted retinas were measured in separate experiments, and no difference was detected between two-month old ASMase$^{+/+}$ (mean ± SD = 487 ± 50 pmol; $n = 4$), ASMase$^{+/-}$ (523 ± 56 pmol, $n = 6$), and ASMase$^{-/-}$ (461 ± 97 pmol, $n = 7$) mice ($P = 0.42$, single factor ANOVA).

NADPH-Generating Capacity of ASMase$^{-/-}$ Mouse Rod Photoreceptors

NADPH is used as a cofactor in the reduction of all-*trans* retinal to all-*trans* retinol in rod photoreceptor outer segments. This reduction reaction then provides a way for measuring the generation of NADPH by the rod photoreceptor cells.[33]

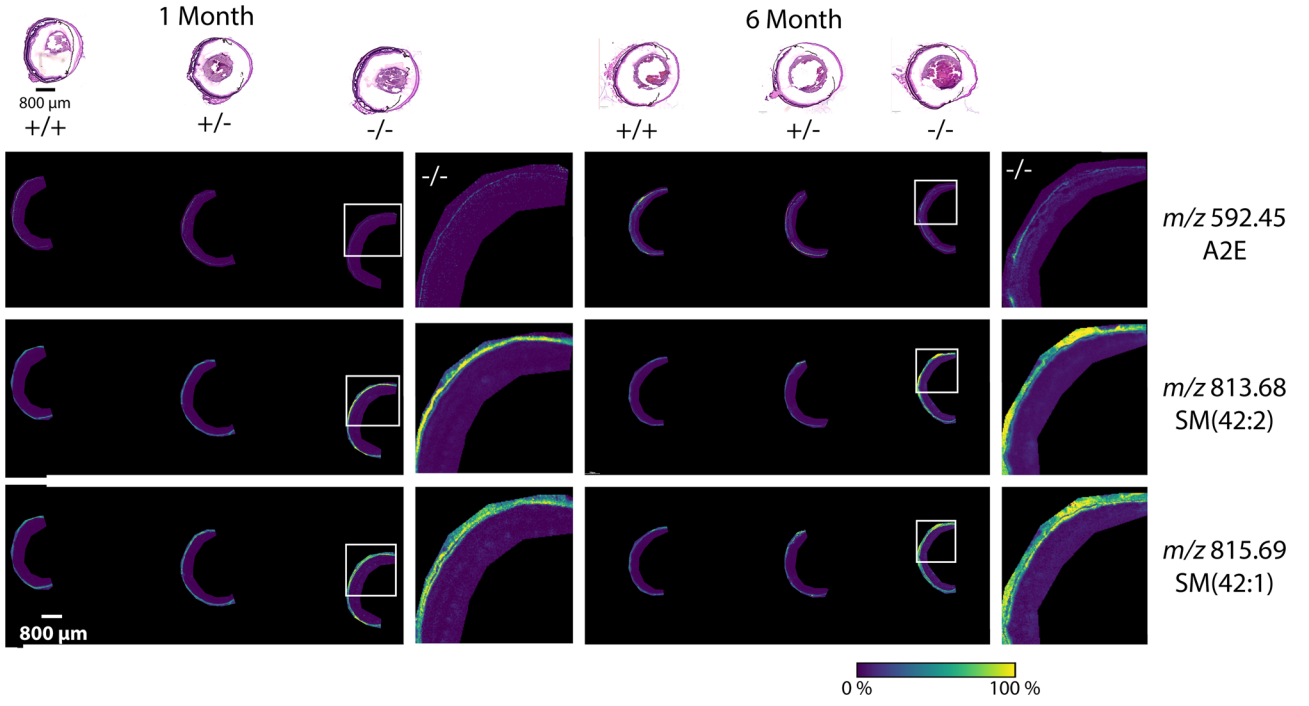

Figure 3. MALDI IMS analysis of ASMase$^{+/+}$, ASMase$^{+/-}$, and ASMase$^{-/-}$ mouse retina tissues in positive ion mode. At the top are the optical images of tissues. MALDI IMS images underneath display the relative abundance of *m/z* 592.45, A2E, *m/z* 813.68, SM (42:2) and *m/z* 815.69, SM (42:1). The **insets** are magnifications of the regions enclosed in the *white squares* showing in detail the distributions in different layers.

Investigative Ophthalmology & Visual Science

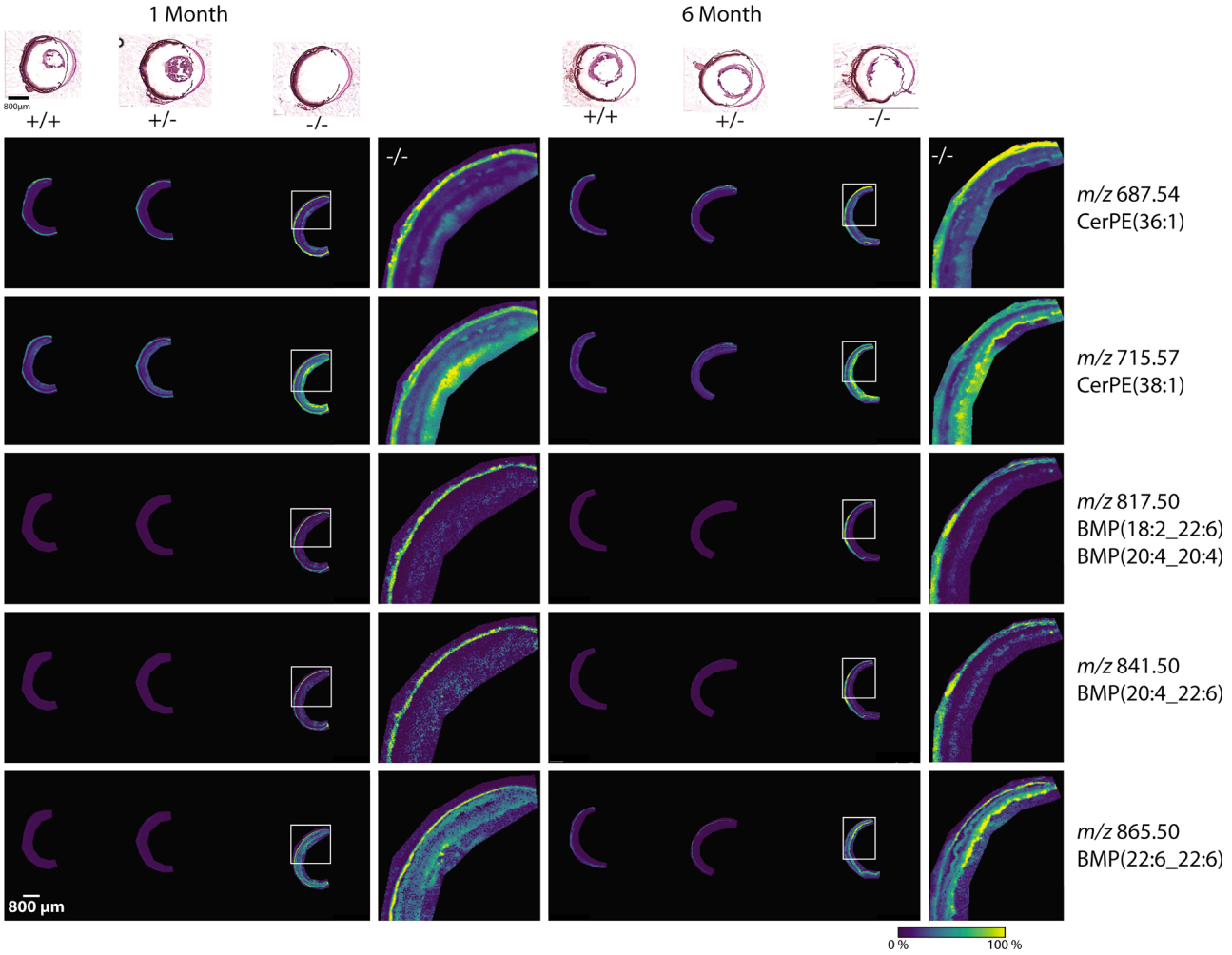

Figure 4. MALDI IMS analysis of ASMase$^{+/+}$, ASMase$^{+/-}$, and ASMase$^{-/-}$ mouse retina tissues in negative ion mode. At the top are the optical images of tissues. MALDI IMS images underneath display the relative abundance of *m/z* 687.54, CerPE (36:1), *m/z* 715.57, CerPE (38:1), *m/z* 817.50, BMP (18:2_22:6), or BMP (20:4_20:4), *m/z* 841.50, BMP (20:4_22:6), and *m/z* 865.50, BMP (22:6_22:6). The insets are magnifications of the regions enclosed in the *white squares* showing in detail the distributions in different layers.

After light excitation of a rod, all-*trans* retinal is released by photoactivated rhodopsin in the outer segment and is reduced to all-*trans* retinol. Because of the large amounts of all-*trans* retinal released by the bleaching of rhodopsin—a mouse rod outer segment contains ~50 million rhodopsin molecules packed at a concentration of ~3 mM[39]—the reduction of all-*trans* retinal reflects the capacity of the rod cell to generate the NADPH required for the reaction. The extent of conversion of all-*trans* retinal to all-*trans* retinol depends on the level of NADPH, that is, the reduced fraction of NADP, and provides a measure of the NADPH-generating capacity of the rod photoreceptor cell. All-*trans* retinal and retinol have similar emission spectra, but their excitation maxima are very different, and the extent of conversion can be measured from the ratio of the intensities of rod outer segment fluorescence excited by 340 and 380 nm (Fex-340/Fex-380).[33] The Fex-340/Fex-380 ratio was measured from different rod cells 30 minutes after the bleaching of rhodopsin, at the time when the outer segment fluorescence reaches its peak value (Fig. 1). As shown in Figure 2, the values of the Fex-340/Fex-380 ratio were not significantly different for wild type and ASMase$^{-/-}$ rod photoreceptors ($P = 0.66$, two-tailed *t*-test), indicating a similar NADPH-generating capacity.

MALDI Imaging of Lipids in the Retina and RPE

Figure 3 shows optical and MALDI IMS images of eye cross sections from one- and six-month old ASMase$^{+/+}$, ASMase$^{+/-}$, and ASMase$^{-/-}$ mice. Selected MALDI IMS images acquired in positive ion mode show increased relative abundance of sphingomyelin species with a C24 N-acyl chain (*m/z* 813.68 and 815.69) in the ASMase$^{-/-}$ RPE and adjacent connective tissue compared to ASMase$^{+/+}$ and ASMase$^{\pm}$ mice (Fig. 3). The increased abundance was observed in both one- and six-month old tissues. No increase in relative abundance in the ASMase$^{-/-}$ RPE was observed for the *bis*-retinoid A2E (*m/z* 592.45), in either one- or six-month old tissues (Fig. 3). Selected MALDI IMS images acquired in negative ion mode are shown in Figure 4. There is increased relative abundance of ceramide-phosphoethanolamine (CerPE) 36:1 (*m/z* 687.54) and 38:1 (*m/z* 715.57) in the ASMase$^{-/-}$ retina and RPE (Fig. 4). Interestingly, for CerPE 36:1 (C18 N-acyl chain)

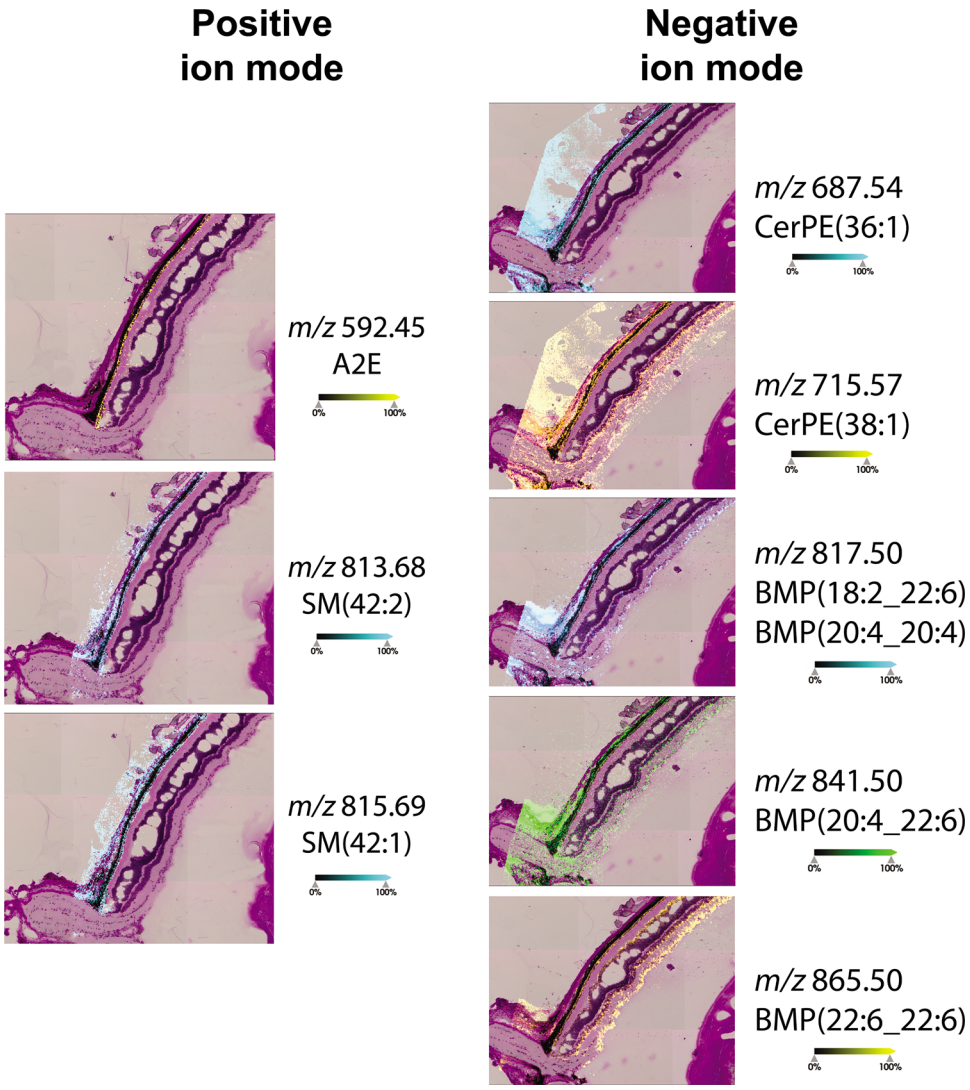

Figure 5. MALDI IMS analysis of six-month-old ASMase$^{-/-}$ mouse retina tissues in positive and negative ion modes at 5 µm resolution. The identified species are the ones shown in Figures 3 and 4. At this resolution, the origins of the signals from specific retinal layers are unequivocally established.

increased relative abundance is observed mainly in the RPE, while for CerPE 38:1 (C20 N-acyl chain) mostly in the inner retina. There is also an increase in the relative abundance of several species of *bis*(monoacylglycero)phosphates (BMPs) (Fig. 4), with *m/z* 817.50 (acyl chains 20:4/20:4 or 18:2/20:6), *m/z* 841.50 (20:4/22:6), and *m/z* 865.50 (22:6/22:6). There are differences in the topography of the relative abundance increase among the different BMP species, with the 22:6/22:6 species showing large increases in the inner retina instead of the RPE.

High resolution localization of the signals from the different species was established with MALDI IMS of 6-month-old ASMase$^{-/-}$ mouse tissue at 5 µm resolution (Fig. 5). From the positive ion mode data, A2E is shown to be strictly localized in the RPE, while the sphingomyelins SM 42:2 and SM 42:1 are found in the RPE, as well as in connective tissue, but not in the choroid. From the negative ion mode data, the ceramide-phosphoethanolamine are both found in the RPE and the connective tissue, with CerPE 38:1 also found in inner retina layers. Similar distributions for these two lipid species have been found in human eye donor tissues (Supplementary Figs. S8 and S9 in[40]). For the BMPs, the distribution of the 22:6/22:6 species is fairly striking, because it is not detected in the connective tissue but is found in the RPE and in abundance in the inner retina. The 20:4/22:6 species is found mainly in the connective tissue and the RPE and can be detected in the inner retina, whereas the *m/z* 817.50 (20:4/20:4 or 18:2/20:6) species are found mostly in connective tissue and are detected in the RPE and in the inner retina as well. As the pixel size for these images is reduced, so is the signal-to-noise ratio in these data, and as a result some signal can be seen in the surrounding areas and off tissue.

Sphingolipid Levels in the Retina and RPE of ASMase$^{-/-}$ Mice

Figure 6 shows the levels of sphingomyelins and ceramides in the retinas and RPEs of 1-, 2- and 6-month old ASMase$^{+/+}$,

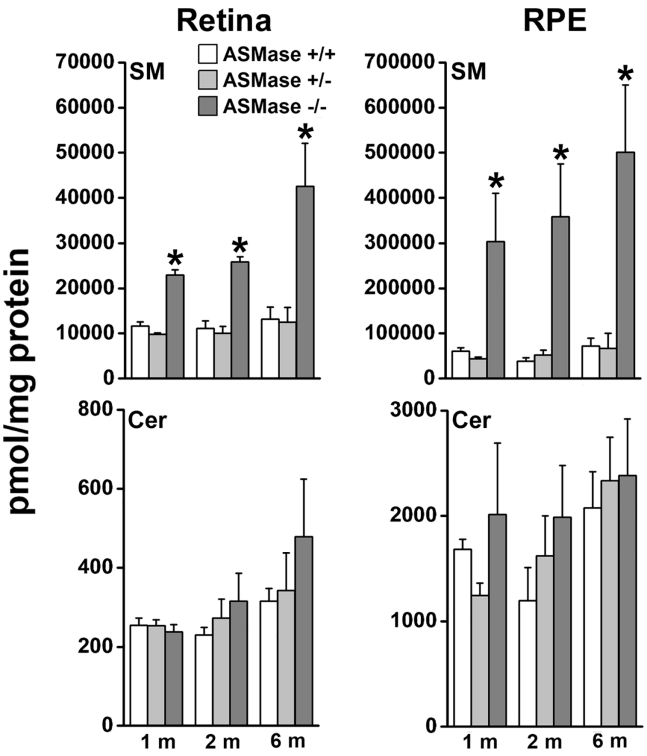

Figure 6. Levels of sphingomyelins (SM) and ceramides (Cer) in the retina and RPE of ASMase$^{+/+}$, ASMase$^{+/-}$, and ASMase$^{-/-}$ mice, at ages of one, two, and six months. For each age and strain, tissue was obtained from $n = 3$ mice and the levels of sphingolipids were determined with LC/MS. *Error bars* represent SD. * indicate statistically significant ($P < 0.017$, adjusted based on Bonferroni correction) difference of ASMase$^{-/-}$ values compared to ASMase$^{+/+}$ and ASMase$^{+/-}$ values, with both differences being statistically significant in all cases.

ASMase$^{+/-}$, and ASMase$^{-/-}$ mice, with the totals representing the sums of the levels of the different acyl chain length species. We analyzed the effects of strain (reflecting the lack of ASMase) and age with two-factor ANOVA. For sphingomyelins, in the retina there was a significant effect of both strain ($P < 0.0001$) and age ($P = 0.002$), while in the RPE only of strain ($P < 0.0001$). Levels of sphingomyelins were the same in ASMase$^{+/+}$ and ASMase$^{+/-}$ animals, but were significantly higher in ASMase$^{-/-}$ mice for all three ages in both the retina and the RPE ($P < 0.017$ for each comparison, one-tailed t-test; significance level was adjusted for multiple comparisons with a Bonferroni correction). For ceramide levels, there was no significant effect of strain in either the retina or RPE ($P = 0.15$ and $P = 0.13$).

In terms of individual sphingolipid species (Fig. 7), there was a significant effect of acyl chain length on prevalence ($P < 0.0001$, two-factor ANOVA), in both retina and RPE, and for all ages. We analyzed in more detail the sphingomyelin species for the two-month old animals with linear regression (excluding the C14 and C26 species, see Methods), finding that in the retina prevalence decreased with acyl chain length for all three strains, ($P < 0.0001$, correlation coefficients $r = 0.86$–0.89). In the RPE, prevalence decreased with acyl chain length for ASMase$^{+/+}$ and ASMase$^{+/-}$ mice ($P = 0.018$ and $r = 0.60$ for both) but not for ASMase$^{-/-}$ animals ($P = 0.30$). For ceramides, prevalence also decreased with acyl chain length in the retina for all three strains ($P = 0.004$–0.009, $r = 0.65$–0.70) but no significant dependence was found in the RPE for any strain ($P > 0.50$ for all).

Discussion

There are several subtypes of Niemann-Pick disease, classified according to affected enzyme, extent of mutations, and disease severity.[7] In humans, the disease due to lack of significant acid sphingomyelinase activity is classified as Niemann-Pick Type A and has the severest phenotype,

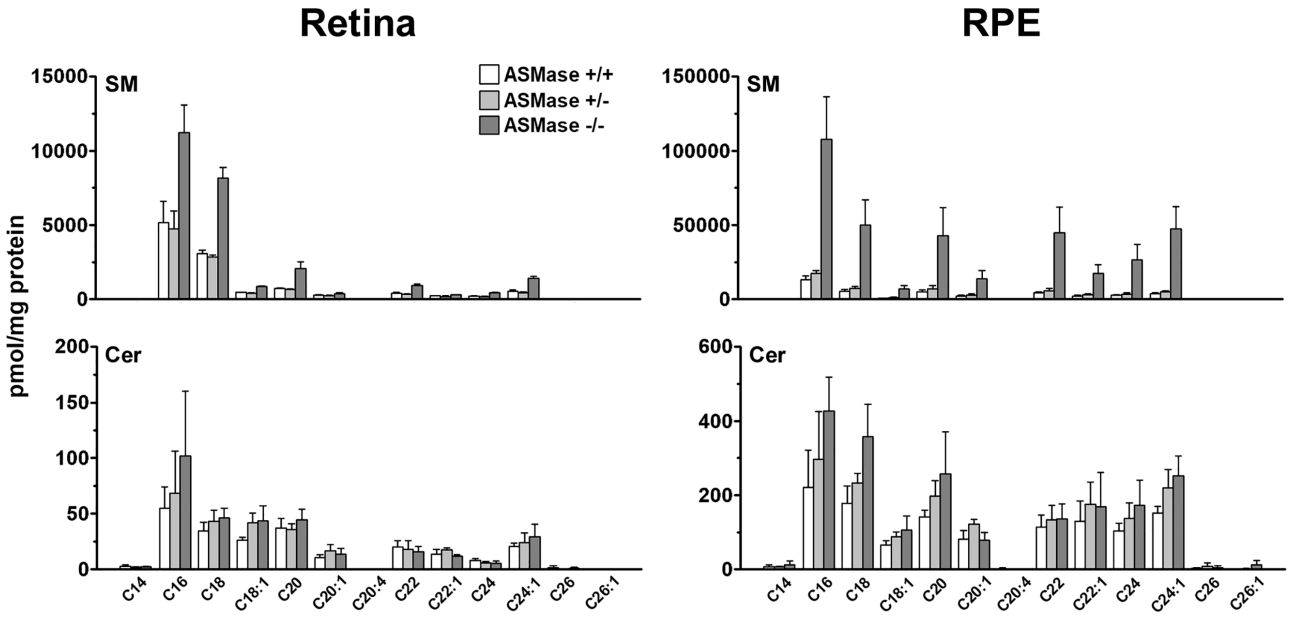

Figure 7. Profiles of sphingomyelins (SM) and ceramides (Cer) of different acyl chain lengths in the retina and RPE of 2 month old ASMase$^{+/+}$, ASMase$^{+/-}$, and ASMase$^{-/-}$ mice. For each strain, tissue was obtained from $n = 3$ mice and the levels of different sphingolipid species were determined with LC/MS. *Error bars* represent *SD*.

Investigative Ophthalmology & Visual Science

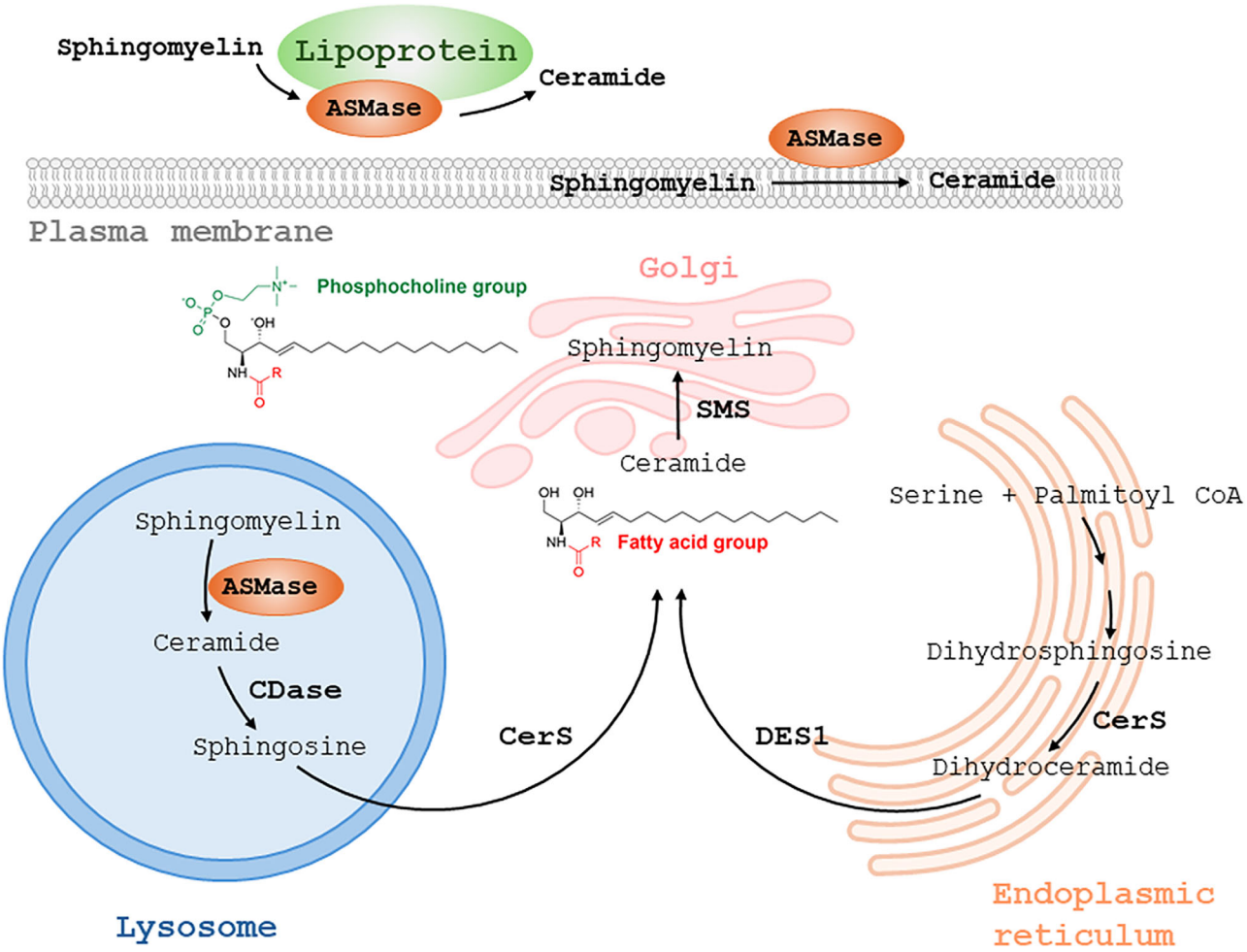

Figure 8. Scheme showing the role of ASMase in sphingolipid metabolism. Lack of the enzyme results in accumulation of sphingomyelin in the lysosomes, as well as in extracellular space. The enzyme plays a central role in sphingolipid recycling and its lack may affect the levels of other sphingolipids in addition to that of its substrate, sphingomyelin. For simplicity, several additional sphingolipid pathways are not shown. ASMase, acid sphingomyelinase; CDase, ceramidase; CerS, ceramide synthase; DES1, dihydroceramide desaturase 1; SMS, sphingomyelin synthase.

resulting in death in early infancy, within two to three years of age.[7,41] One of its ocular manifestations is a macular cherry-red spot that appears by 12 months of age[42] and is the result of a perimacular halo.[43] The changes in retinal appearance are thought to be the result of lipid accumulation in the lysosomal compartments of different retinal cells,[44] an interpretation supported by the studies of the ASMase$^{-/-}$ mouse model of the disease, showing large accumulation of sphingomyelin in the retina and RPE and of lipofuscin in RPE cells.[8]

Mice that lack ASMase exhibit significant reduction in ERG amplitude and retinal degeneration that progress with age.[8] We surmised that the lysosomal dysfunction caused by the lack of ASMase, and evidenced by the accumulation of sphingomyelin (Fig. 6) and lipofuscin, as well as by the reduction in ERG amplitude, would also impair other metabolic processes. To examine the potential impact of the lack of ASMase on rod photoreceptor metabolism and the processing of the retinyl chromophore, we used 2-month old animals in order to minimize interference by age-dependent degenerative changes. Surprisingly, neither the kinetics of all-*trans* retinol formation after the bleaching of rhodopsin nor the NADPH-generating capacity of rod photoreceptors were affected by the lack of ASMase (Figs. 1, 2). Although metabolic limitations can result in reduced NADPH-generating capacity, the results of Figure 2 do not exclude the presence of metabolic impairments in ASMase$^{-/-}$ mouse retinas that are not manifested as reduced NADPH availability. Lack of ASMase does not affect the passive removal of all-*trans* retinol (Fig. 1), which suggests that the changes in sphingolipid metabolism do not appear to affect plasma membrane structure.

Impairment in the reduction of all-*trans* retinal to all-*trans* retinol will result in the accumulation of all-*trans* retinal and increased formation of *bis*-retinoid lipofuscin precursors in rod outer segments.[16,45] Thus the lack of an effect of ASMase deficiency on the formation of all-*trans* retinol is consistent with the similar abundance of the *bis*-retinoid A2E in the RPE of ASMase$^{-/-}$ and ASMase$^{+/+}$ mice (Fig. 3). By contrast, compared to wild type (ASMase$^{+/+}$), ASMase$^{-/-}$ retinas and RPEs show large increases in the abundance of sphingomyelins and CerPE (Figs. 3, 4). There are also large increases in the abundance of several BMP species (Fig. 4) that have been associated with lysosomal

dysfunction.[29–31] Large increases in the abundance of these BMP species were also observed in the RPE of *Abca4*$^{-/-}$ mice,[46] indicative of a lysosomal dysfunction, which in that case was caused by the excessive accumulation of *bis*-retinoids such as A2E. It is important to note that in the RPE of *Abca4*$^{-/-}$ animals no increase in the abundance of sphingomyelin species was observed in our previous study[46] (data not shown). Figures 3 and 4 also show the differential accumulation of ASMase substrates in different retinal layers, which would indicate the cell-specific regulation of individual sphingolipid species. Interestingly, as confirmed by the high resolution MALDI IMS images (Fig. 5), ASMase substrates (sphingomyelins and ceramide phosphoethanolamines) accumulate specifically in the connective tissue layer between choroid and sclera, which may reflect the loss of the secreted form of ASMase, a product of the same gene as the lysosomal enzyme.[47] Differential accumulation across retinal layers was observed for different BMP species as well (Figs. 4 and 5), again pointing to cell-specific prevalence of the precursors of individual species. The distribution of the increases in the levels of different sphingolipids in ASMase$^{-/-}$ mice does not correlate with the pattern of ASMase expression in the retina, with highest expression found in the inner layers,[48] thereby pointing to significant contributions from additional enzymes and pathways of sphingolipid metabolism.

In ASMase$^{-/-}$ animals, and in contrast to the large increases in sphingomyelins, the substrate of ASMase, no major changes were observed in the levels of ceramides (Fig. 6), the product of sphingomyelin hydrolysis by ASMase.[49] One possibility is that in the absence of ASMase there are compensatory increases in ceramide synthesis that could maintain ceramide levels. Figure 8 (based on reference 50) provides a simplified overview of the pathways, lysosomal and extracellular, that involve ASMase. ASMase can act on sphingomyelin in the lysosomes, in the extracellular leaflet of the plasma membrane, or in lipoproteins present in extracellular space. Lack of ASMase will result in the accumulation of sphingomyelin in the lysosomes as well as in extracellular space. The lack of a significant decrease in ceramide levels may be due to a compensatory increase in synthesis.

In agreement with previous reports,[8] we find that C16 and C18 are the dominant sphingomyelin species in the retina, as well as in the RPE, though in the latter's case longer chain species are more prominent than in the retina. The same pattern was observed in ASMase$^{-/-}$ retinas, again, with longer chain sphingomyelin species being more prominent in the RPE. For all three strains, the acyl chain patterns of sphingomyelins and ceramides are different between sphingolipid types and between retina and RPE (Fig. 7), pointing to individual regulation of different sphingolipid species, as also suggested by the MALDI imaging analysis.

In summary, we find that lack of ASMase results in the increased accumulation of sphingomyelins and ceramide phosphoethanolamines, as well as in the increased abundance of BMPs, lipid species indicative of lysosomal dysfunction. Contrary to our expectations, the lysosomal dysfunction associated with the lack of ASMase does not affect the formation of all-*trans* retinol and the availability of NADPH in rod photoreceptors, or the abundance of the *bis*-retinoid A2E in the RPE. Our results suggest that, at least at younger ages, the pathology caused by the lack of ASMase progresses without affecting the processing of the retinyl chromophore and the generation of NADPH in rod photoreceptors.

Acknowledgments

Supported by a Medical University of South Carolina College of Medicine Enhancement of Team Science award (JF and YK) and National Eye Institute grant R01 EY014850 (YK). YK is the Barbara and Stanley Andrie Endowed Chair for Bioengineering and Vision Research in the Vision SmartState Center of Economic Excellence.

Disclosure: **B. Rahman**, None; **D.M.G. Anderson**, None; **C. Chen**, None; **J. Liu**, None; **L.G. Migas**, None; **R. Van de Plas**, None; **K.L. Schey**, None; **M. Kono**, None; **J. Fan**, None; **Y. Koutalos**, None

References

1. Katz ML, Robison WG, Jr. What is lipofuscin? Defining characteristics and differentiation from other autofluorescent lysosomal storage bodies. *Arch Gerontol Geriatr*. 2002;34:169–184.
2. Terman A, Brunk UT. Lipofuscin. *Int J Biochem Cell Biol*. 2004;36:1400–1404.
3. Feeney L. Lipofuscin and melanin of human retinal pigment epithelium. Fluorescence, enzyme cytochemical, and ultrastructural studies. *Invest Ophthalmol Vis Sci*. 1978;17:583–600.
4. Sparrow JR, Boulton M. RPE lipofuscin and its role in retinal pathobiology. *Exp Eye Res*. 2005;80:595–606.
5. Futerman AH, van Meer G. The cell biology of lysosomal storage disorders. *Nat Rev Mol Cell Biol*. 2004;5:554–565.
6. Toledano-Zaragoza A, Ledesma MD. Addressing neurodegeneration in lysosomal storage disorders: Advances in Niemann Pick diseases. *Neuropharmacology*. 2020;171:107851.
7. Schuchman EH, Desnick RJ. Types A and B Niemann-Pick disease. *Mol Genet Metab*. 2017;120:27–33.
8. Wu BX, Fan J, Boyer NP, et al. Lack of Acid Sphingomyelinase Induces Age-Related Retinal Degeneration. *PLoS One*. 2015;10:e0133032.
9. Adler IV L, Boyer NP, Chen C, Ablonczy Z, Crouch RK, Koutalos Y. The 11-cis retinal origins of lipofuscin in the retina. *Prog Mol Biol Transl Sci*. 2015;134:e1–12.
10. Kim HJ, Sparrow JR. Novel bisretinoids of human retina are lyso alkyl ether glycerophosphoethanolamine-bearing A2PE species. *J Lipid Res*. 2018;59:1620–1629.
11. Sparrow JR, Gregory-Roberts E, Yamamoto K, et al. The bisretinoids of retinal pigment epithelium. *Prog Retin Eye Res*. 2012;31:121–135.
12. Eldred GE, Lasky MR. Retinal age pigments generated by self-assembling lysosomotropic detergents. *Nature*. 1993;361:724–726.
13. Parish CA, Hashimoto M, Nakanishi K, Dillon J, Sparrow J. Isolation and one-step preparation of A2E and iso-A2E, fluorophores from human retinal pigment epithelium. *Proc Natl Acad Sci USA*. 1998;95:14609–14613.
14. Finnemann SC, Leung LW, Rodriguez-Boulan E. The lipofuscin component A2E selectively inhibits phagolysosomal degradation of photoreceptor phospholipid by the retinal pigment epithelium. *Proc Natl Acad Sci USA*. 2002;99:3842–3847.
15. Lakkaraju A, Finnemann SC, Rodriguez-Boulan E. The lipofuscin fluorophore A2E perturbs cholesterol metabolism in retinal pigment epithelial cells. *Proc Natl Acad Sci USA*. 2007;104:11026–11031.
16. Ben-Shabat S, Parish CA, Vollmer HR, et al. Biosynthetic studies of A2E, a major fluorophore of retinal pigment epithelial lipofuscin. *J Biol Chem*. 2002;277:7183–7190.
17. Boyer NP, Higbee D, Currin MB, et al. Lipofuscin and N-retinylidene-N-retinylethanolamine (A2E) accumulate in the

retinal pigment epithelium in the absence of light exposure: their origin is 11-Cis retinal. *J Biol Chem*. 2012;287:22276–22286.

18. Boyer NP, Thompson DA, Koutalos Y. Relative contributions of all-trans and 11-Cis retinal to formation of lipofuscin and A2E accumulating in mouse retinal pigment epithelium. *Invest Ophthalmol Vis Sci*. 2021;62:1.
19. Quazi F, Molday RS. ATP-binding cassette transporter ABCA4 and chemical isomerization protect photoreceptor cells from the toxic accumulation of excess 11-cis-retinal. *Proc Natl Acad Sci USA*. 2014;111:5024–5029.
20. Ebrey T, Koutalos Y. Vertebrate photoreceptors. *Prog Retin Eye Res*. 2001;20:49–94.
21. Wald G. Molecular basis of visual excitation. *Science*. 1968;162:230–239.
22. Lamb TD, Pugh EN, Jr. Dark adaptation and the retinoid cycle of vision. *Prog Retin Eye Res*. 2004;23:307–380.
23. Saari JC. Biochemistry of visual pigment regeneration: the Friedenwald lecture. *Invest Ophthalmol Vis Sci*. 2000;41:337–348.
24. Okajima TI, Pepperberg DR, Ripps H, Wiggert B, Chader GJ. Interphotoreceptor retinoid-binding protein promotes rhodopsin regeneration in toad photoreceptors. *Proc Natl Acad Sci USA*. 1990;87:6907–6911.
25. Chen C, Thompson DA, Koutalos Y. Reduction of all-trans-retinal in vertebrate rod photoreceptors requires the combined action of RDH8 and RDH12. *J Biol Chem*. 2012;287:24662–24670.
26. Maeda A, Maeda T, Imanishi Y, et al. Role of photoreceptor-specific retinol dehydrogenase in the retinoid cycle in vivo. *J Biol Chem*. 2005;280:18822–18832.
27. Rattner A, Smallwood PM, Nathans J. Identification and characterization of all-trans-retinol dehydrogenase from photoreceptor outer segments, the visual cycle enzyme that reduces all-trans-retinal to all-trans-retinol. *J Biol Chem*. 2000;275:11034–11043.
28. Futterman S, Hendrickson A, Bishop PE, Rollins MH, Vacano E. Metabolism of glucose and reduction of retinaldehyde in retinal photoreceptors. *J Neurochem*. 1970;17:149–156.
29. Jabs S, Quitsch A, Kakela R, et al. Accumulation of bis(monoacylglycero)phosphate and gangliosides in mouse models of neuronal ceroid lipofuscinosis. *J Neurochem*. 2008;106:1415–1425.
30. Rouser G, Kritchevsky G, Knudson AG, Jr., Simon G. Accumulation of a glycerolphospholipid in classical niemann-pick disease. *Lipids*. 1968;3:287–290.
31. Walkley SU, Vanier MT. Secondary lipid accumulation in lysosomal disease. *Biochim Biophys Acta*. 2009;1793:726–736.
32. Horinouchi K, Erlich S, Perl DP, et al. Acid sphingomyelinase deficient mice: a model of types A and B Niemann-Pick disease. *Nat Genet*. 1995;10:288–293.
33. Adler IV L, Chen C, Koutalos Y. Mitochondria contribute to NADPH generation in mouse rod photoreceptors. *J Biol Chem*. 2014;289:1519–1528.
34. Chen C, Blakeley LR, Koutalos Y. Formation of all-trans retinol after visual pigment bleaching in mouse photoreceptors. *Invest Ophthalmol Vis Sci*. 2009;50:3589–3595.
35. Ala-Laurila P, Kolesnikov AV, Crouch RK, et al. Visual cycle: dependence of retinol production and removal on photoproduct decay and cell morphology. *J Gen Physiol*. 2006;128:153–169.
36. Wu Q, Blakeley LR, Cornwall MC, Crouch RK, Wiggert BN, Koutalos Y. Interphotoreceptor retinoid-binding protein is the physiologically relevant carrier that removes retinol from rod photoreceptor outer segments. *Biochemistry*. 2007;46:8669–8679.
37. Koutalos Y, Ebrey TG, Tsuda M, et al. Regeneration of bovine and octopus opsins in situ with natural and artificial retinals. *Biochemistry*. 1989;28:2732–2739.
38. Spraggins JM, Djambazova KV, Rivera ES, et al. High-performance molecular imaging with MALDI trapped ion-mobility time-of-flight (timsTOF) mass spectrometry. *Anal Chem*. 2019;91:14552–14560.
39. Lem J, Krasnoperova NV, Calvert PD, et al. Morphological, physiological, and biochemical changes in rhodopsin knockout mice. *Proc Natl Acad Sci USA*. 1999;96:736–741.
40. Anderson DMG, Messinger JD, Patterson NH, et al. Lipid landscape of the human retina and supporting tissues revealed by high-resolution imaging mass spectrometry. *J Am Soc Mass Spectrom*. 2020;31:2426–2436.
41. Graber D, Salvayre R, Levade T. Accurate differentiation of neuronopathic and nonneuronopathic forms of Niemann-Pick disease by evaluation of the effective residual lysosomal sphingomyelinase activity in intact cells. *J Neurochem*. 1994;63:1060–1068.
42. Walton DS, Robb RM, Crocker AC. Ocular manifestations of group A Niemann-Pick disease. *Am J Ophthalmol*. 1978;85:174–180.
43. Rudich DS, Curcio CA, Wasserstein M, Brodie SE. Inner macular hyperreflectivity demonstrated by optical coherence tomography in niemann-pick disease. *JAMA Ophthalmol*. 2013;131:1244–1246.
44. Robb RM, Kuwabara T. The ocular pathology of type A Niemann-Pick disease. A light and electron microscopic study. *Invest Ophthalmol*. 1973;12:366–377.
45. Adler IV L, Chen C, Koutalos Y. All-trans retinal levels and formation of lipofuscin precursors after bleaching in rod photoreceptors from wild type and Abca4(−/−) mice. *Exp Eye Res*. 2017;155:121–127.
46. Anderson DMG, Ablonczy Z, Koutalos Y, et al. Bis(monoacylglycero)phosphate lipids in the retinal pigment epithelium implicate lysosomal/endosomal dysfunction in a model of Stargardt disease and human retinas. *Sci Rep*. 2017;7:17352.
47. Schissel SL, Schuchman EH, Williams KJ, Tabas I. Zn2+-stimulated sphingomyelinase is secreted by many cell types and is a product of the acid sphingomyelinase gene. *J Biol Chem*. 1996;271:18431–18436.
48. Fan J, Liu J, Liu J, et al. Sphingomyelinases in retinas and optic nerve heads: Effects of ocular hypertension and ischemia. *Exp Eye Res*. 2022;224:109250.
49. Marchesini N, Hannun YA. Acid and neutral sphingomyelinases: roles and mechanisms of regulation. *Biochem Cell Biol*. 2004;82:27–44.
50. Jenkins RW, Canals D, Hannun YA. Roles and regulation of secretory and lysosomal acid sphingomyelinase. *Cell Signal*. 2009;21:836–846.

Investigative Ophthalmology & Visual Science